

Preparation of dysprosium carbonate and dysprosium oxide efficient photocatalyst nanoparticles through direct carbonation and precursor thermal decomposition

Mehdi Rahimi-Nasrabadi^{1,2} · Seied Mahdi Pourmortazavi³ · Mohammad Reza Ganjali^{4,5} · Parviz Novrouzi⁴ · Farnoosh Faridbod⁴ · Meisam Sadeghpour Karimi³

Received: 29 July 2016 / Accepted: 20 October 2016 / Published online: 9 November 2016
© Springer Science+Business Media New York 2016

Abstract Dysprosium carbonate nanoparticles were prepared through a direct precipitation method using $\text{Dy}(\text{NO}_3)_3$ and Na_2CO_3 as a facile, well-regulated and cost-effective technique for the production insoluble salts. Due to the importance of improving the capability and quality of a process for adjusting the size of the product particles the optimal precipitation reaction parameters were evaluated through the Taguchi method. The reaction conditions like the concentrations of the reacting species, the rate of the addition of the reagent as well as the reactor temperature were also optimized based on an orthogonal array design. It was concluded from the results that dysprosium carbonate nanoparticles can be synthesized through the direct carbonation process by controlling the concentration of carbonate ion, the rate of its addition to the reactor and the reaction temperature. Further, a one-step thermal decomposition method was used for the efficient conversion of dysprosium carbonate to dysprosium oxide nanoparticles. The characterization of the products was

carried out through XRD, SEM, TEM, FT-IR and thermal analysis techniques. Furthermore, the as-synthesized dysprosium carbonate and dysprosium oxide nanoparticles were used as photocatalyst for the photocatalytic degradation of methylene orange under ultraviolet light.

1 Introduction

Synthesis and applications of nanomaterials have attracted a great deal of attention, due to the exclusive physical and chemical properties they possess, due to the fact that particle sizes as low as a few nanometers can lead to changes in the properties of a substance [1–9].

In recent years, environmental issues have been extensively investigated and special attention has been paid to the area of photocatalysis due to the high applicability of these compounds [10–13]. In this area, the decolorization of organic dyes such as methylene blue (MB), rhodamine B (RhB) and methyl orange is of great value because the discharge of these compounds from industrial plants causes severe adverse effects to the environment and greatly increases the water pollution effectively disturbing the ecosystem [14, 15].

Oxides of rare-earth elements, on the other hand, have extensive applications in high-performance luminescent devices, magnets, catalysts, and other functional materials based on the electronic, optical, and chemical characteristics arising from their 4f electrons [16–18]. Among rare earth ions, Dy(III) is well known as an activating dopant in diverse inorganic lattices, producing white light emission [17]. Furthermore, Dy^{3+} can act as a sensitive probe ion due to the fluorescence properties originating from its 5d–4f transition and also the effects of the crystal fields on its 5d state [18]. Mixtures and alloys of lanthanides have also

✉ Mehdi Rahimi-Nasrabadi
kpmrahimi@ihu.ac.ir; rahiminasrabadi@gmail.com

✉ Seied Mahdi Pourmortazavi
poumortazavi@yahoo.com

¹ Faculty of Pharmacy, Baqiyatallah University of Medical Sciences, Tehran, Iran

² Department of Chemistry, Imam Hossein University, Tehran, Iran

³ Faculty of Material and Manufacturing Technologies, Malek Ashtar University of Technology, Tehran, Iran

⁴ Center of Excellence in Electrochemistry, University of Tehran, Tehran, Iran

⁵ Endocrinology & Metabolism Research Center, Tehran University of Medical Sciences, Tehran, Iran

been used in high quality hard and soft magnets [19]. Nanoscale magnetic materials have further been used in ferrofluids, high density magnetic storages and as performance permanent magnets, high frequency electrical applications, etc. [20]. The oxides of rare earth elements (e.g. dysprosium, samarium, erbium, yttrium, europium, and lutetium) can find other prominent applications like use in dielectric multilayer ceramic capacitors (MLCC), high efficiency phosphors, and catalysis [21–23].

Dysprosium sesquioxide, Dy_2O_3 , is an alkaline, highly insoluble, and thermally stable material [24], with high electrical resistivity, large energy bands, and a high dielectric constant [25]. The salt takes a cubic crystal structure below 1870 °C and monoclinic and/or hexagonal structures above this temperature [26]. The basic properties of Dy_2O_3 depend on the nature of the precursor used for its preparation, as well as the pretreatment conditions, and the salt can have been used for glass, optic, and ceramic applications [27], further to its applications as a dopant in fluorescent and glass materials with a Faraday rotation effect for optical and laser-based devices, luminescence, magneto-optical recording materials, materials with a large magnetostriction, measurement of neutron energy-spectrum, nuclear reaction control rods, neutron absorbers, glass additives, and rare earth permanent magnets [28–30]. Paramagnetic lanthanide oxide nanoparticles (PLONs) reveal a range of magnetic and optical characteristics due to the 4f electrons in the three valent cations [31, 32], which make them excellent candidates for use as magnetic resonance (MR) and/or optical imaging agents. PLONs reveal lower unsaturated magnetizations in comparison to superparamagnetic iron oxide nanoparticles (SIONs) which show almost saturated magnetizations of >40 emu/g in clinical MR fields in ambient temperature [33]. The magnetization of PLONs have also been proven to be size-independent (5–10 emu/g) at room temperature while that of SIONs has been reported to drop upon reducing particle dimensions [34]. Among the lanthanide ions, Dy(III) and Ho(III) cations have the maximum magnetic moments [35], turning their nano-structures to promising alternatives for use in T2 MR imaging with renal excretion.

Reports on the preparation of Dy(III) compounds range from the use of hydro- or solvo-thermal [36, 37], and sol-gel approaches [24] to other methods [29, 30]. Xu et al. prepared $\text{Dy}(\text{OH})_3$ and Dy_2O_3 nanotubes through the hydrothermal method [16]. A hydrothermal process at 130 and 210 °C, was reported for the preparation of dysprosium hydroxide and oxide nanorods from commercial bulk Dy_2O_3 crystals [38]. Regarding the prominence and widespread applications of nanoscale particles of Dy_2O_3 with controlled morphology, there is always great desire for cost effective methods.

In the light of the above mentioned, this work was intended to optimize a facile and cost-effective method for

the preparation of high-purity nano-sized particles of dysprosium carbonate which can be used for the large scale production of this compound. This was achieved through the direct precipitation reaction of $\text{Dy}(\text{NO}_3)_3 \cdot 6\text{H}_2\text{O}$ and Na_2CO_3 in an aqueous media. In order to be able to optimize the synthesis route, an experimental design procedure was used to examine the effect of the different experimental parameters on the dimensions of the product. The evaluated parameters included the concentration of Dy(III) and carbonate ions, the flow rate of the cation solution and the temperature of the reactor.

Subsequently, thermal analysis was used to monitor the weight changes and thermal events during the dehydration and decomposition processes and the results were used to gain important evidence on the calcination of dysprosium carbonate, which leads to its decomposition into single-dispersed nanocrystalline Dy_2O_3 . Finally, methyl orange (MO) degradation in the presence of the nano-particles was used to evaluate the catalytic behavior of the carbonate and oxide nano-particles.

2 Experimental

2.1 Materials and apparatus

Reagent grade dysprosium nitrate, sodium carbonate and ethanol were used as received from Merck. Scanning electron micrographs (SEM) were recorded on a Philips XL30 series instrument using a gold film for loading the dried particles on the instrument. Gold films were prepared by a sputter coater model SCD005, BAL-TEC (Switzerland). X-ray powder diffraction (XRD) studies were performed using a Rigaku D/max 2500 V diffractometer equipped with a graphite monochromator and a Cu target. The IR spectra were obtained on an IR spectrophotometer (Bruck Equinox 55) using the KBr pellet technique. Transmission electron microscope (TEM) images were acquired with a Zeiss-EM900 SEM. The sample was coated on a Cu-carbon coated grid prior to the measurement. Thermogravimetric (TG) and differential thermal analyses (DTA) were performed on 5 mg of the sample using a Stanton Redcroft STA-780 series and an alumina crucible. The operating conditions of the analysis included incremental heating at the rate of 10 °C/min in the range of 25–780 °C, in an inert atmosphere of nitrogen blown at 50 mL/min. The UV-Vis diffuse reflectance spectra were recorded at room temperature using an Avantes Spectrometer, Avaspec-2048-TEC.

2.2 Optimization of the synthesis procedure

To synthesize the nanoparticles, Dy(III) solutions with several concentrations were added to carbonate solutions,

under vigorous stirring at various reactor temperatures and flow rates. Once the precipitation reaction was complete, the product was filtered and washed with distilled water three times, before being washed with ethanol twice. Next the nanoparticles were dried at 80 °C for 4 h.

To optimize the experimental parameters influencing the reaction (i.e. concentration of the dysprosium and carbonate ion solutions, flow rate of the dysprosium solution, and the temperature of the reactor temperature) as shown in Table 1, an experimental design approach was used.

2.3 Synthesis of Dy₂O₃ nanoparticles through thermal decomposition

Dy₂O₃ was prepared through the thermal decomposition of the dysprosium carbonate, which was obtained as described above under the optimum conditions. The dysprosium carbonate was heated in a furnace under an air atmosphere at 650 °C for 3 h. To this end, 0.5 g of the precursor were loaded into the reactor without being pressed into an alumina crucible (30 mm in diameter and 14 mm height).

2.4 Diffuse reflectance spectroscopy (DRS)

The diffuse reflectance data was used to measure the optical band gap energy of dysprosium carbonate and dysprosium oxide nanoparticles. The optical band gap energy is specified as the minimum photon energy required to excite an electron from the valence band to conduction band of a semiconductor. The energy dependence of semiconductors absorption edge is given by Tauc’s equation [39–41]:

$$\alpha h\nu = A(h\nu - E_g)^{\eta} \tag{1}$$

where h , ν , α , E_g , A are Planck’s constant, frequency of light, absorption coefficient, band gap energy and a proportional constant, respectively. The value of the exponent

η is $\frac{1}{2}$ and 2 for direct and indirect transitions respectively. In this study the value of η was $\frac{1}{2}$ for both dysprosium carbonate and oxide nanoparticles.

2.5 Photocatalytic activity

The photocatalytic activities of the as-synthesized dysprosium carbonate and dysprosium oxide nanoparticles were evaluated by using them in the photo-degradation of methyl orange (MO) under UV irradiation. A cylindrical Pyrex double pipe air-lift photoreactor was used in the experiments, and the UV irradiation was carried out using a high pressure Hg lamp (250 W, $\lambda > 254$ nm) positioned inside a quartz pipe centered inside of the reactor.

The reaction suspension was prepared by adding 0.05 g of the photocatalytic nano-particles (0.1 g/L) into 500 mL of the aqueous solution of MO (5 mg/L). Prior to the irradiation, the suspension was magnetically stirred in the dark for 20 min to reach the adsorption equilibrium. The above suspensions containing the synthesized dysprosium carbonate and dysprosium oxide nano-particles were subjected to ultraviolet light separately under constant aeration. Both before and at various time intervals during the illumination phase (i.e. at 0, 10, 20, 30 and 40 min) samples were taken from reactor, centrifuged and analyzed by a UV–Vis spectrometer at the maximum absorption wavelength of MO. During the experiments the temperature was kept constant at 25 °C by cooling the reactor.

The Lambert–Beer law, which describes relationship between concentration of a solution (C) and the absorbance of light (A) in a solution is:

$$A = \epsilon bC \tag{2}$$

In this equation A , ϵ , b and C are the absorbance of light, molar absorptivity, path length of the sample and the concentration of pollutant in solution, respectively. If A and A_0 are used to show the obtained absorbance at t and

Table 1 OA₉ (3⁴) experimental design and mean particle size of produced dysprosium carbonate as results

Trial number	Dy ³⁺ conc. (mol/L)	CO ₃ ²⁻ conc. (mol/L)	Dy ³⁺ feed flow rate (mL/min)	Temperature (°C)	Diameter of dysprosium carbonate particles (nm)
1	0.01	0.01	2.5	0	30
2	0.01	0.03	10	30	40
3	0.01	0.09	40	60	48
4	0.03	0.01	10	60	38
5	0.03	0.03	40	0	35
6	0.03	0.09	2.5	30	40
7	0.09	0.01	40	30	38
8	0.09	0.03	2.5	60	36
9	0.09	0.09	10	0	42

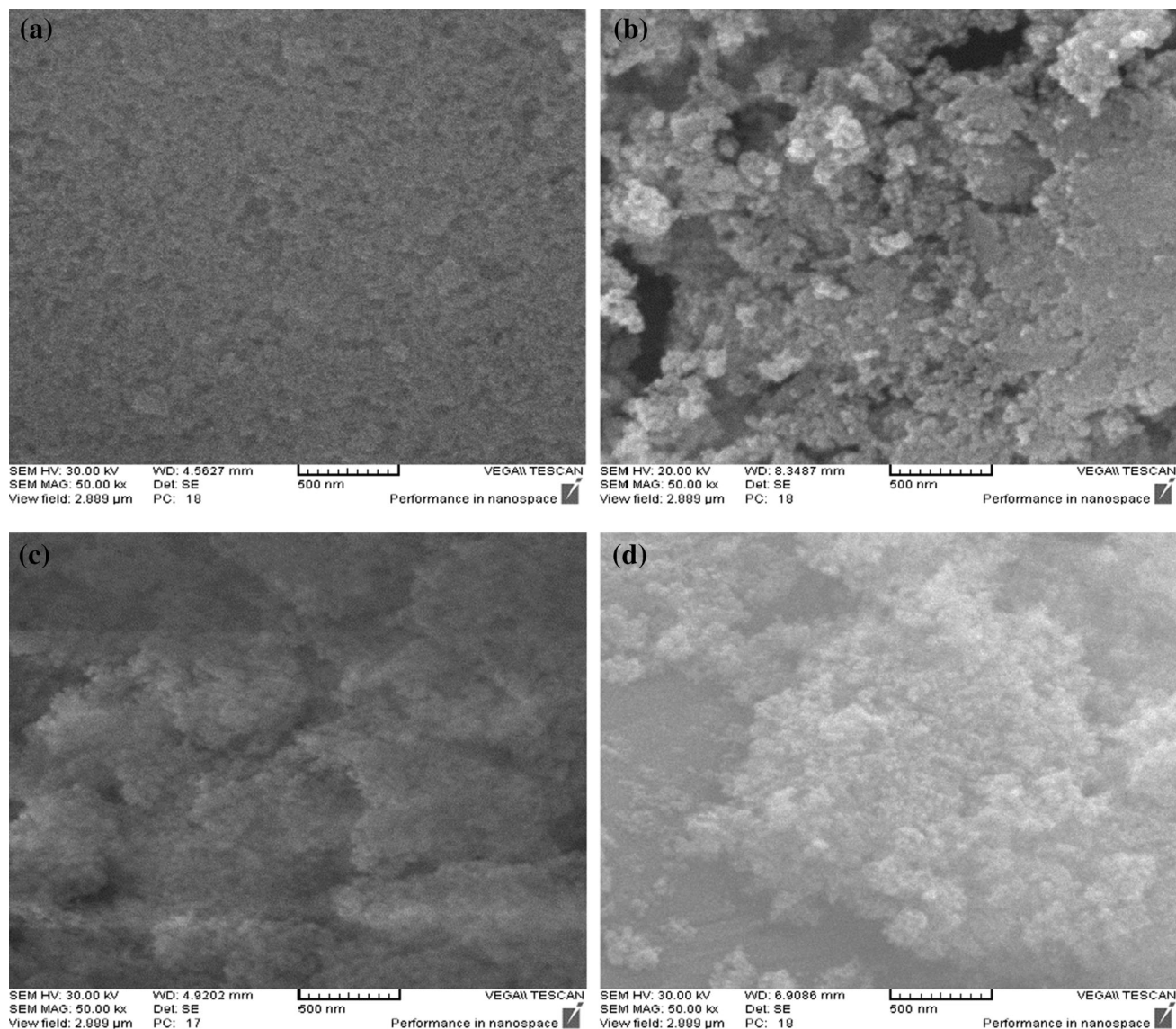


Fig. 1 SEM images of dysprosium carbonate superstructures obtained at different runs, presented in Table 1, by direct carbonation according experimental condition: **a** run 1, **b** run 4, **c** run 6 and **d** run 8

0 min from the onset of the reaction and C_t and C_0 show the corresponding MO concentrations, one can write the below relations:

$$\frac{A}{A_0} = \frac{C}{C_0} \quad (3)$$

and

$$\text{Degradation efficiency (\%)} = \frac{A_0 - A_t}{A_0} \times 100 \quad (4)$$

The photocatalytic degradation kinetics of the photo-degradation reaction was studied based on the Langmuir–Hinshelwood model, which is commonly used for the photocatalytic degradation of organic molecules at low concentrations. The model is expressed as [40]:

$$-\frac{dC}{dt} = k_{app}C \quad (5)$$

where C , k_{app} , t and $-\frac{dC}{dt}$ represent the concentration of MO, reaction rate constant, time and reaction rate, respectively.

3 Results and discussion

3.1 Synthesis of dysprosium carbonate and its optimization through OAD

Precipitation of a salt through mixing the anion and cation solutions is a common route that has been used for the

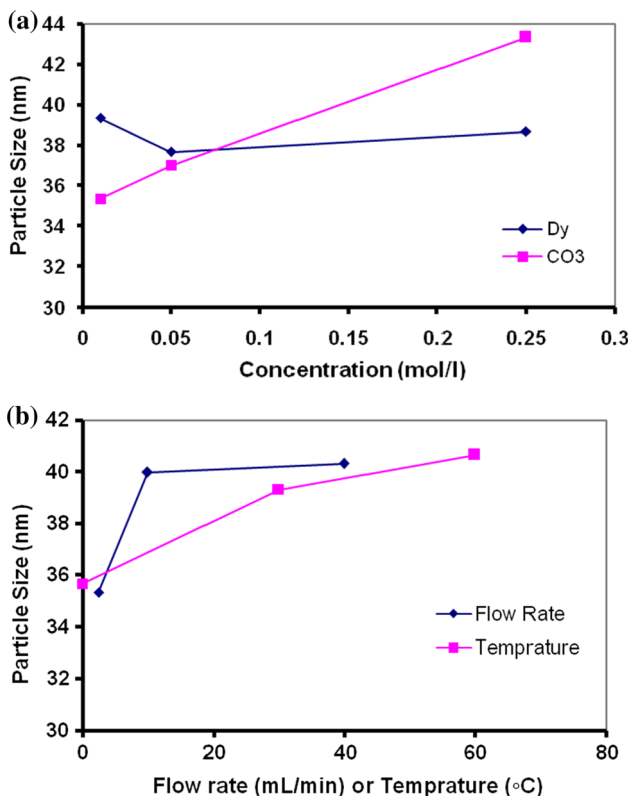


Fig. 2 Main effects for each variable at various levels on the size of dysprosium carbonate nanoparticles

synthesis of several water insoluble inorganic materials like dysprosium carbonate [41, 42]. Controlling the size and shape of the particles, however, can be a rather complex task, which requires a fundamental understanding of the interactions between reagents. Here we attempted to determine how the various parameters affect the precipitation process and hence the properties of the dysprosium carbonate nanoparticles, through a Taguchi orthogonal array design [43, 44]. The method was used to select the most prominent parameters influencing the particle size and particle size distribution of the product. Table 1 illustrates the structure of the Taguchi orthogonal array design and the results of the measurements. The factors studied included the concentrations of dysprosium and

Table 2 Results of ANOVA for dysprosium carbonate nanoparticles synthesis using direct carbonation procedure by OA₉(3⁴) matrix

Factor	Code	DOF	S	V	Pooled ^a			
					DOF	\bar{S}	\bar{F}	\bar{P}^a
Dysprosium concentration (mol/L)	Dy	2	4.2	2.1	–	–	–	–
Carbonate concentration (mol/L)	CO ₃	2	106.9	53.4	2	106.9	25.3	51.8
Flow rate (mL/min)	F	2	46.9	23.4	2	46.9	11.1	21.5
Temperature (°C)	T	2	40.2	20.1	2	40.2	9.5	18.2
Error	E	–	–	–	2	4.2	–	8.5

The critical value was at 90 % confidence level; pooled error results from pooling of insignificant effect

^a Percentage of contribution

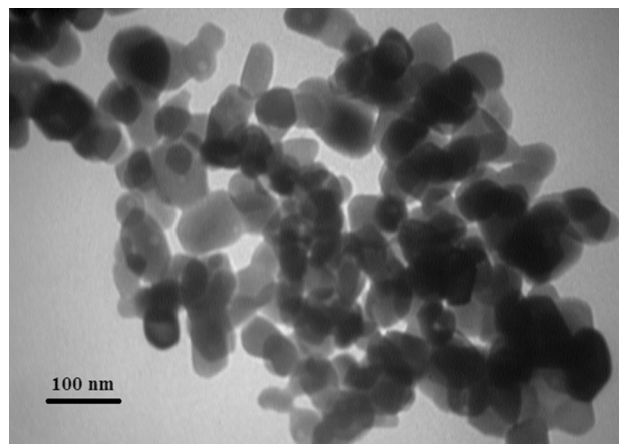


Fig. 3 TEM image of dysprosium carbonate nanoparticles obtained under optimum conditions

carbonate solutions, the flow rate of the cation solution, and the reactor temperature. SEM images of four dysprosium carbonate samples obtained through the method are illustrated in Fig. 1.

Since the experimental design was orthogonal, it was possible to separate the effect of each control factor at diverse levels through averaging the responses at each level. The mean particle size values of the factors at each level were calculated according to the assignment of the experiment (Fig. 2). Actually the calculation of the average dysprosium carbonate particle sizes corresponding to each factor, e.g. the effect of the concentration of the carbonate solution at level 1 (0.01 M), was carried out through summing the particle size of the products in experiments where carbonate concentration was set at level 1 (runs 1, 4 and 7) and dividing the result by the number of trials at this level. The normal value for each level (of each factor), revealed how the particle size of the product changed upon varying the level.

Using the analysis of variance (ANOVA), which is a method of investigating the significance of the in affecting a characteristic quality (here the dimensions of dysprosium carbonate), and considering the variables as independent from one another, the optimum conditions, the influence of

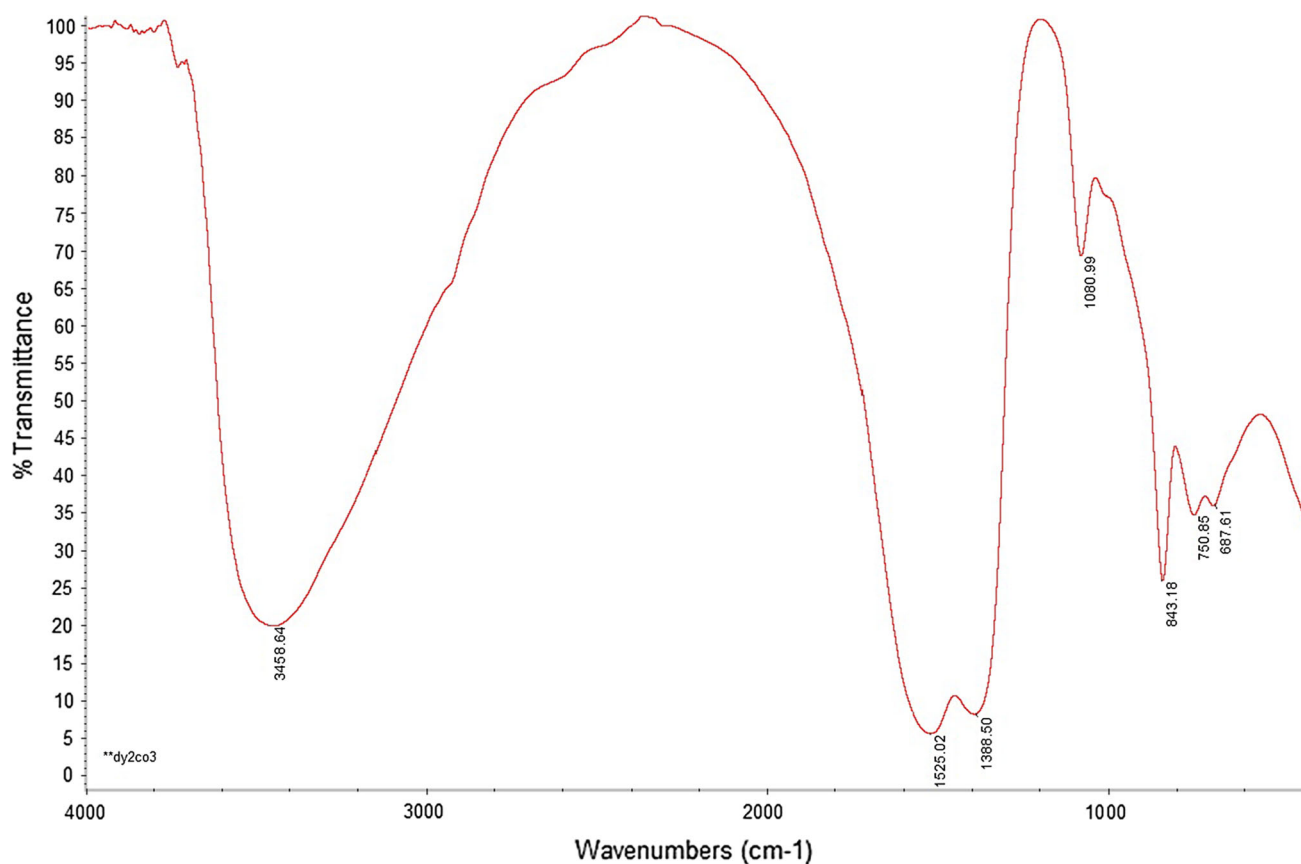


Fig. 4 FT-IR spectra of the precipitated dysprosium carbonate nanoparticles obtained under optimum conditions

each factor at different levels, and the particle size of the optimal product were determined. The results of the ANOVA of the effect of different parameters on the dimensions of the dysprosium carbonate nanoparticles are summarized in Table 2, where S and V represent the sum of the square of each variable or error term, and the variance of the results for each parameter respectively. These results can be used to evaluate the degree a control factor affects

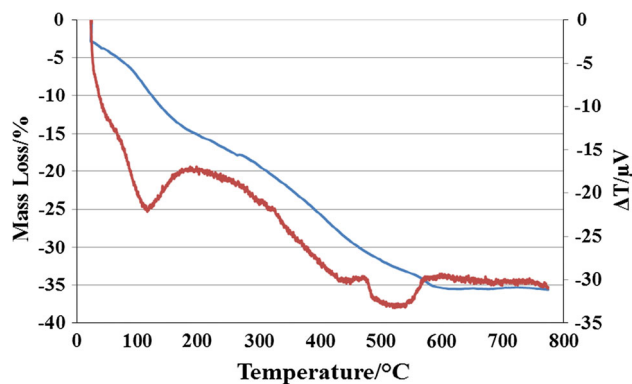


Fig. 5 TG/DTG/DTA curves for thermal decomposition reaction of dysprosium carbonate precursor; sample mass 5.0 mg; heating rate 10 °C/min; nitrogen atmosphere

the characteristics of the particle size, or in other words, the significance of the control factors on the particle size using the F values of the F -distribution. F values are used to determine if a control factor can be pooled to an error term or not. The results of the experiments generally have a small degree of freedom, and hence a pooling procedure is used to increase the freedom of error [45, 46].

The effects of the concentrations of dysprosium and carbonate ions on the particle size of the product were investigated at three different levels (i.e. 0.01, 0.03 and 0.09 mol/L) and it was observed that the concentration of Dy(III) was not a significant parameter in this regard. However, the concentration of the carbonate ion was found to be an important factor influencing the dimensions of the product. Further the influence of the reactor temperature on the dimensions of the produced dysprosium carbonate nanoparticles was studied at the three levels (i.e. 0, 30 and 60 °C) and it was observed that this significantly affects the size of the product.

The flow rates at which the cation solutions were added to the anion solutions, were also investigated and it was observed that it significantly influences the size of the dysprosium carbonate particles. The results of ANOVA on these experiments showed that at a 90 % confidence level,

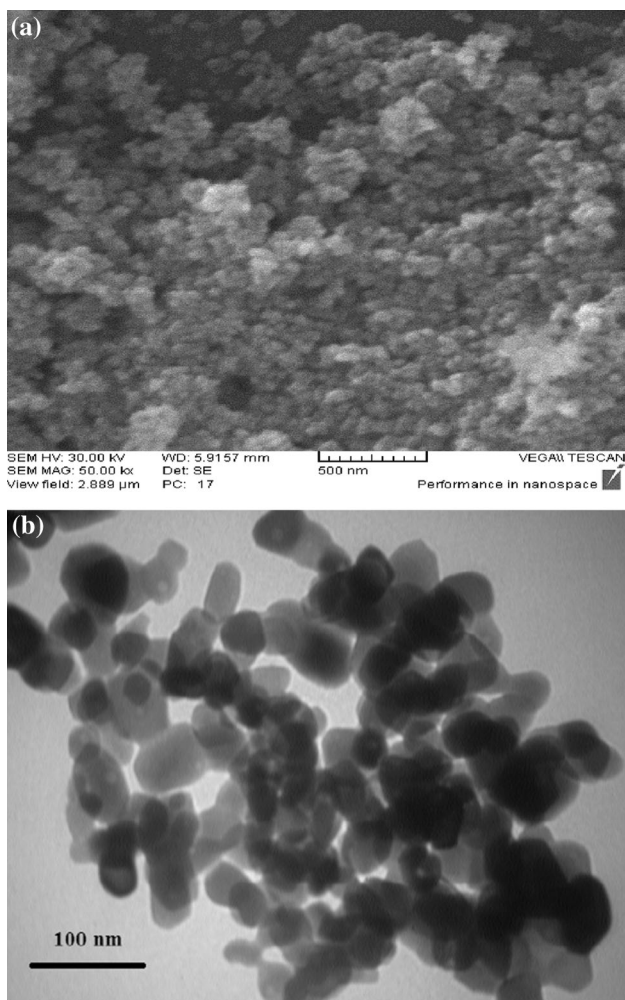


Fig. 6 **a** SEM image and **b** TEM image of dysprosium oxide nanoparticles obtained from thermal decomposition reaction of precursor

all parameters except for the concentration of the dysprosium solution have substantial effects on the dimensions of the particles. As already mentioned the possible interactions among the variables were not considered.

The ANOVA results indicated 0.01 mol/L to be the optimum carbonate concentration for preparing the dysprosium carbonate nanoparticles of desired dimensions. Also a flow rate of 2.5 mL/min for the dysprosium solution a temperature of 0 °C were determined as optimal.

The optimal result of the procedure can be calculated using the following equation based on the Taguchi experimental design [47, 48]:

$$Y_{opt} = \frac{T}{N} + \left(C_x - \frac{T}{N} \right) + \left(F_y - \frac{T}{N} \right) + \left(Tem_z - \frac{T}{N} \right)$$

In this equation, T/N is the average diameter of the product particles (T being the sum of all results, and N being the total number of results in Table 1); Y_{opt} is the diameter of

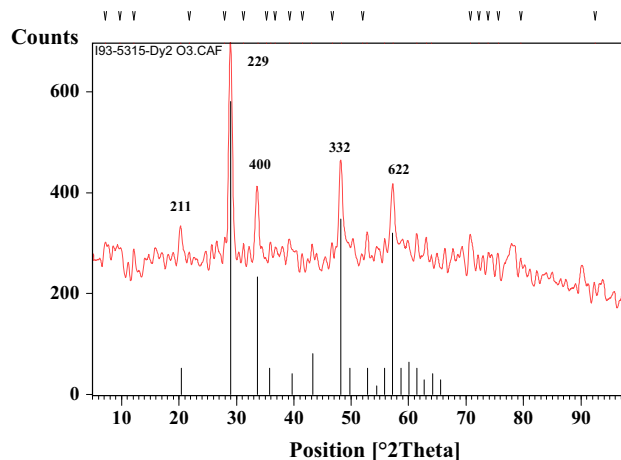


Fig. 7 XRD pattern of the dysprosium oxide prepared by thermal decomposition reaction of precursor

the particles prepared under the best conditions; and C_x , F_y , and Tem_z represent the optimal CO_3^{2-} concentration, flow rate, and temperature, respectively. On the other hand, under optimal conditions, the confidence interval (C.I.) of the dimensions of the product can be calculated by the following expression [49]:

$$CI = \pm \sqrt{\frac{F_\alpha(f_1, f_2) V_e}{N_e}}$$

where, $F_\alpha(f_1, f_2)$ is the F value from an F table at the degrees of freedom (DOF) f_1 and f_2 at the level of significance α (in this work, $\alpha = 90$), $f_1 = DOF$ of mean (which always equals 1), $f_2 = DOF$ of the pooled error term, N_e effective number of replications, and is given by $N_e = \text{number of trials} / (\text{DOF of mean (always equals 1)} + \text{total DOF of factors used for the prediction})$. Calculations for the prediction of the particle size of product under optimal conditions and CI for the calculated particle dimensions revealed that at a confidence level of 90 %, the size of the product nanoparticles are 29 ± 4 nm.

As indicated in the first run of Table 1, the optimum synthesis conditions resulted by ANOVA were 0.01 mol/L for carbonate ion solution, 2.5 mL/min for the flow rate of dysprosium solution, and 0 °C for the temperature [50].

The SEM results showed that the particles prepared under the conditions of run 1 have an average diameter of about 30 nm (Fig. 1a), which falls in the range estimated for the particle under the optimal conditions. The size and morphology of the sample particles were further characterized by TEM (Fig. 3), the results of which were consistent with those obtained SEM, indicating that the dysprosium carbonate particles prepared under optimal conditions were spherical with an average diameter of about 30 nm. Thus, the nanoparticles synthesized under the

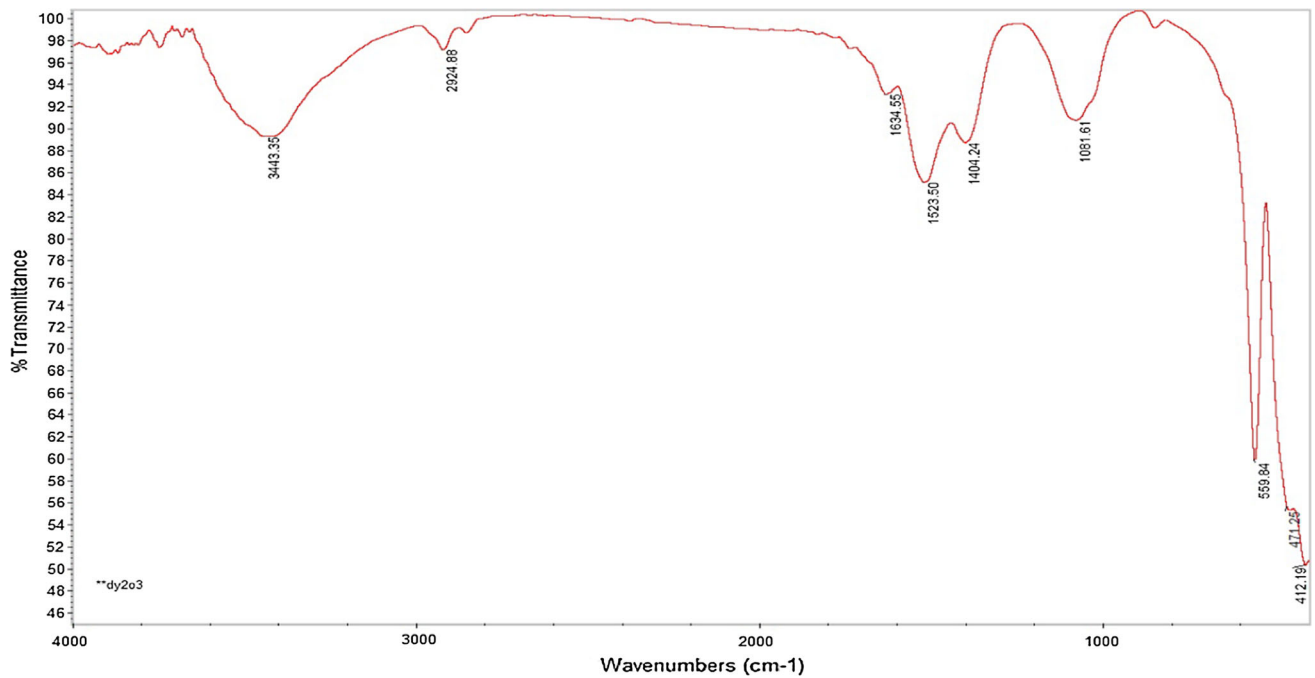


Fig. 8 FT-IR spectra of the dysprosium oxide nanoparticles obtained by thermal decomposition reaction of precursor

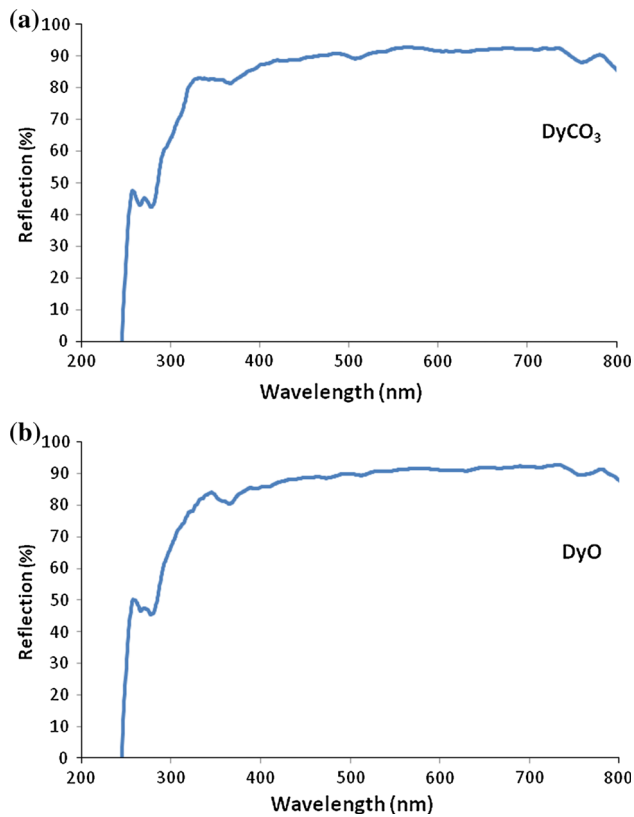


Fig. 9 Diffuse reflectance UV-Vis spectra of as-synthesized, **a** dysprosium carbonate (DyCO_3) and **b** dysprosium oxide (DyO) nanoparticles

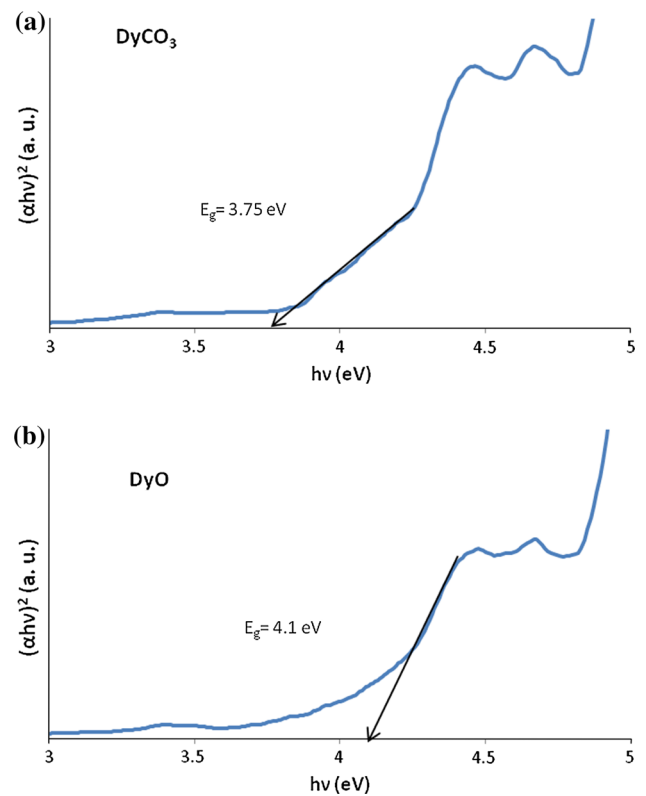


Fig. 10 Tauc's plot for as-prepared **a** dysprosium carbonate (DyCO_3) and **b** dysprosium oxide (DyO) nanoparticles

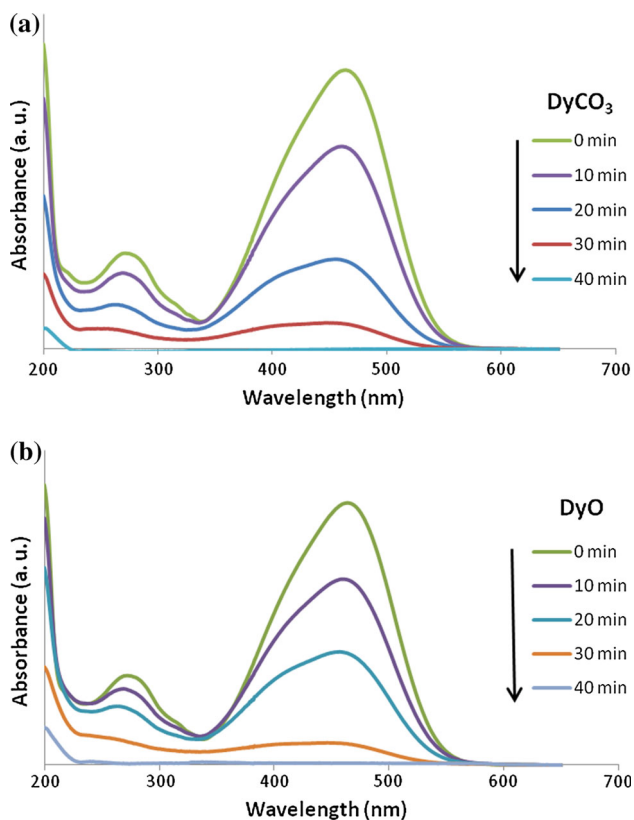


Fig. 11 UV–Vis absorbance spectrum of MO at different time intervals on irradiation using 0.1 g/L, **a** dysprosium carbonate (DyCO_3) and **b** dysprosium oxide (DyO) nanoparticles as photocatalyst

conditions of run 1, were treated as the optimal product and studied by FT-IR and thermal analysis techniques.

3.2 Characterization of the optimum product

Regarding the ability of FT-IR spectroscopy in the analysis of the functional groups, the IR spectra of dried precipitate prepared under optimum conditions, were obtained and a sample is illustrated in Fig. 4. The absorption peak at 3458.6 cm^{-1} in this spectrum corresponds to the stretching vibration of the O–H bond, as well as the bending vibration of H–O–H absorbed on the outer surface of the sample in the course of handling the sample before obtaining the spectra [41–43]. The absorption bands at 1525 and 1388 cm^{-1} could be attributed to the ν_3 mode of CO_3^{2-} group. The splitting of the bands could be due to the inhomogenous crystallographic environment of the carbonate ions. The four absorption bands at 1081, 843, 751 and 688 cm^{-1} were also assigned to the stretching vibrations of carbonate ions [29, 30].

The thermoanalytical graphs of dysprosium carbonate nanoparticles acquired under the best conditions are

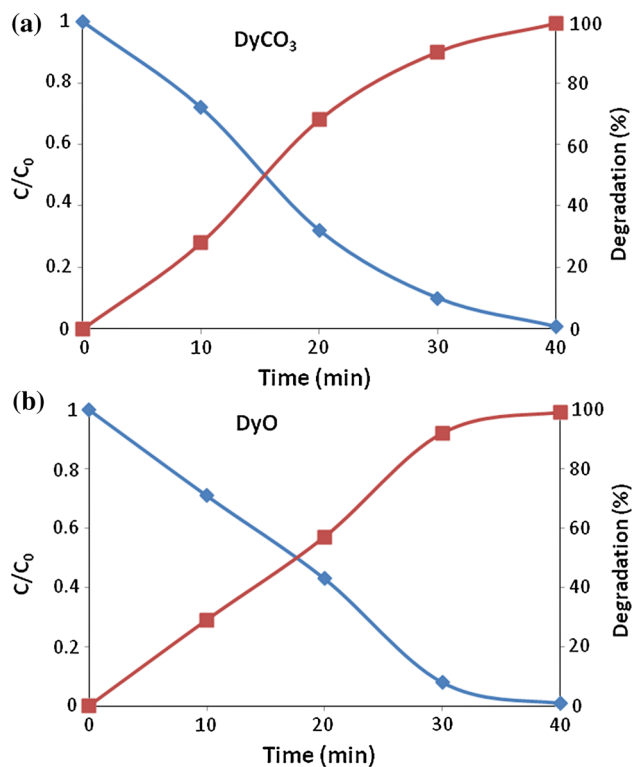


Fig. 12 Photocatalytic degradation of MO solution under UV irradiation using, **a** dysprosium carbonate (DyCO_3) and **b** dysprosium oxide (DyO) nanoparticles as photocatalyst

Table 3 Pseudo first order reaction rate constant and conversion efficiency of photocatalysis at 40 min

	K (min^{-1})	Conversion (%)
Dysprosium carbonate	0.097	99.3
Dysprosium oxide	0.0931	99

illustrated in Fig. 5. The TG–DTA graphs, obtained in a nitrogen atmosphere, revealed that dysprosium carbonate experiences two major mass losses. The first step occurred in the range of 40–190 °C, due to the elimination of the surface-adsorbed H_2O and equals about 15 % of the weight of the sample, and the was witnessed in the range of 200–600 °C, and was attributed to the OH^- and CO_3^{2-} from the basic dysprosium carbonate particles. The DTA curve during the second step revealed another broad endothermic peak at about 500 °C, indicating that OH^- and CO_3^{2-} are lost simultaneously. Except for this endothermic peak and that attributed to the moisture loss, no other peaks were observed in the DTA curve, indicating that the precursor undergoes only one major decomposition. The mass of the carbonate sample after 600 °C, was approximately constant which could be held as proof that dysprosium carbonate completely decomposed into

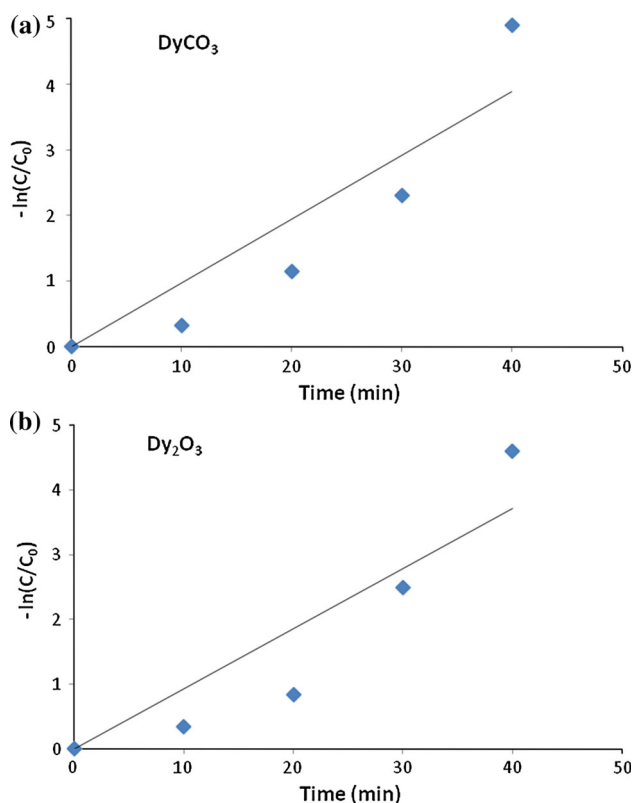


Fig. 13 Pseudo first order kinetics of MB degradation for, **a** dysprosium carbonate (DyCO_3) and **b** dysprosium oxide (Dy_2O_3) nanoparticles

dysprosium oxide in the former stage. So, $650\text{ }^\circ\text{C}$ was considered as the optimum temperature for the calcination of the product.

3.3 Decomposition of dysprosium carbonate into dysprosium oxide

Based on the results of the TG–DTA analyses on the dysprosium carbonate nanoparticles, a thermal decomposition treatment was used to prepare dysprosium oxide at $650\text{ }^\circ\text{C}$. The SEM and TEM images of the product which were obtained in the course of the method, are presented in Fig. 6. Figure 6a shows the average size of dysprosium oxide particles to be about 48 nm, which is consistent with the results obtained from the TEM image of the sample (Fig. 6b).

Figure 7 illustrates the XRD patterns of the dysprosium oxide nanoparticles. The high intensity and smooth baseline of the pattern indicated the product to have a high purity crystalline structure. All of the diffraction peaks in this figure are in compliance with the cubic system structure of dysprosium oxide from PDF card 00-009-0197.

Figure 8 shows an IR spectrum of the dysprosium oxide samples obtained by the calcination of the carbonate precursor at $650\text{ }^\circ\text{C}$ for 3 h. The result are in complete accord with Refs. [29, 30] and indicate the formation of the highly pure dysprosium oxide. By comparing the IP spectra of the precursor (Fig. 4) and the product (Fig. 8), it was observed that the absorption peak at 3458 cm^{-1} , which originates from the stretching vibration of hydrogen bonds due to the abundance of the hydroxyl group in the precursor is significantly reduced in Fig. 8. This is indicative of the complete elimination of the hydroxyl groups from the sample after the calcination step. After heating the sample up to $650\text{ }^\circ\text{C}$, the absorption band of carbonate ions at 1525 and 1388.5 cm^{-1} were also diminished while those corresponding to the cubic phase of Dy_2O_3 at 559.8 , 471.3 and 412.2 cm^{-1} (Fig. 8) strengthened.

Figure 9a, b shows the a UV–Vis diffuse reflectance spectrum (DRS) of the prepared nanoparticles and Fig. 10a, b shows Tauc's plot for the dysprosium carbonate and dysprosium oxide nanoparticles. As shown, the estimated band gaps for this samples are around 3.75 and 4.1 eV. This reveals an absorption edge of around 331 and 302 nm for dysprosium carbonate and oxide nanoparticles respectively.

3.4 Photodegradation of methyl orange

As shown in Fig. 11 the photocatalytic activities of the optimal dysprosium carbonate and oxide nanoparticles were monitored to evaluate their photodegradation performance. Figure 12 shows the changes in the concentration of the test MO solution in the presence of dysprosium carbonate and oxide nanoparticles upon UV irradiation as plots of the C/C_0 and degradation efficiency versus illumination time. It was found that the degradation of MO occurs in the presence of dysprosium carbonate and oxide nanoparticles. After 40 min the maximum conversions were reached which equalled about 99.3 and 99 % for dysprosium carbonate and oxide, respectively.

Figure 13 indicates the pseudo first-order kinetics plot of MO degradation in the presence of dysprosium carbonate and oxide nanoparticles. The slope of the linear regression gives the first-order reaction rate constant. The rate constants and maximum conversions of the photocatalysis are summarized in Table 3, and these results indicate that nanoparticles of both dysprosium carbonate and oxide have good ability to eliminate organic pollutants.

The results suggested that dysprosium carbonate and oxide are superior species which might constitute helpful and effective photocatalysis for purification of water from organic pollutants.

4 Conclusion

The precipitation method was tested and optimized for the preparation of dysprosium carbonate nanoparticles. The technique proved to be a controllable route for the synthesis of dysprosium carbonate nanoparticles in aqueous media at low temperatures. The optimization of the reaction parameters was performed using the Taguchi robust design. The result showed that the composition of the carbonate ion, the flow rate of the Dy(III) solutions and the reactor temperature have substantial effects on the particle size of the product. The carbonate particles prepared under the optimal conditions were about 30 nm in diameter. Further thermal studies showed that dysprosium carbonate undergoes a single stage decomposition to form dysprosium oxide particles with an average size of about 48 nm. The optimized methods for the preparation of dysprosium carbonate and oxide nanoparticles revealed several advantages, including simplicity, low cost, high output and good product purity, in addition to producing superfine products that can be prepared in large scales. Applying dysprosium carbonate and oxide nanoparticles, as the photocatalyst led to the respective degradation yields of 99.3 and 99 % for MO after 40 min irradiation of UV light.

References

1. F. Ahmadi, M. Rajabi, F. Faizi, M. Rahimi-Nasrabadi, B. Maddah, *Int. J. Environ. Anal. Chem.* **94**, 1123 (2014)
2. A. Ziarati, J. Safaei-Ghomi, S. Rohani, *Chin. Chem. Lett.* **24**, 195 (2013)
3. V. Arabali, M. Ebrahimi, M. Abbasghorbani, V. Kumar Gupta, M. Farsi, M.R. Ganjali, F. Karimi, *J. Mol. Liq.* **213**, 312 (2016)
4. M. Amiri, H. Salehniya, A. Habibi-Yangjeh, *Ind. Eng. Chem. Res.* **55**, 8114 (2016)
5. B. Maddah, S.S. Javadi, A. Mirzaei, M. Rahimi-Nasrabadi, *J. Liq. Chromatogr. Relat. Technol.* **38**, 208 (2015)
6. H.R. Naderi, M.R. Ganjali, A. Shiralizadeh Dezfali, P. Norouzi, *RSC Adv.* **6**, 51211 (2016)
7. H.R. Naderi, M.R. Ganjali, P. Norouzi, *Int. J. Electrochem. Sci.* **11**, 4267 (2016)
8. J. Tizfahm, M. Aghazadeh, M. Ghannadi Maragheh, M.R. Ganjali, P. Norouzi, F. Faridbod, *Mater. Lett.* **167**, 153 (2016)
9. M. Rahimi-Nasrabadi, S.M. Pourmortazavi, M.R. Ganjali, A.R. Banan, F. Ahmadi, *J. Mol. Struct.* **1074**, 85 (2014)
10. M. Pirhashemi, A. Habibi-Yangjeh, *J. Colloid Interface Sci.* **474**, 103 (2016)
11. B. Golzad-Nonakaran, A. Habibi-Yangjeh, *Adv. Powder Technol.* **27**, 1427 (2016)
12. S. Vadivel, D. Maruthamani, B. Paul, S.S. Dhar, A. Habibi-Yangjeh, S. Balachandran, B. Saravanakumar, A. Selvakumar, K. Selvam, *RSC Adv.* **6**, 74177 (2016)
13. A. Akhundi, A. Habibi-Yangjeh, *Mater. Chem. Phys.* **174**, 59 (2016)
14. S. Vadivel, D. Maruthamani, A. Habibi-Yangjeh, B. Paul, S.S. Dhar, K. Selvam, *J. Colloid Interface Sci.* **480**, 126 (2016)
15. A.-W. Xu, Y.-P. Fang, L.-P. You, H.-Q. Liu, *J. Am. Chem. Soc.* **125**, 1494 (2003)
16. J.L. Sommerdijk, A. Bril, *J. Electrochem. Soc.* **122**, 952 (1975)
17. M. Rahimi-Nasrabadi, M. Behpour, A. Sobhani-Nasab, S.M. Hosseinpour-Mashkani, *J. Mater. Sci.: Mater. Electron.* **26**, 9776 (2015)
18. J.P. Jakubovics, *Magnetism and Magnetic Materials* (Cambridge University Press, Cambridge, 1994)
19. A. Joseph, G.L. Praveen, K. Abha, G.M. Lekha, S. George, *J. Lumin.* **132**, 1999 (2012)
20. H. Kishi, Y. Mizuno, H. Chazono, *Jpn. J. Appl. Phys.* **42**, 1 (2003)
21. R.P. Rao, *J. Electrochem. Soc.* **143**, 189 (1996)
22. S. Eridie, R. Roy, *Mater. Res. Bull.* **30**, 145 (1995)
23. T. Sreethawong, S. Chavadej, S. Ngamsinlapasathian, S. Yoshikawa, *J. Colloid Interface Sci.* **300**, 219 (2006)
24. T.-M. Pan, W.-T. Chang, F.-C. Chiu, *Appl. Surf. Sci.* **257**, 3964 (2011)
25. P. Kofstad, *Nonstoichiometry, Diffusion, and Electrical Conductivity in Binary Metal Oxide* (Wiley, New York, 1972)
26. K. Tanabe, K. Mismo, Y. Ono, H. Hattori, *New Solid Acids and Bases* (Elsevier, New York, 1989)
27. M. Chandrasekhar, D.V. Sunitha, N. Dhananjaya, H. Nagabhushana, S.C. Sharma, B.M. Nagabhushana, C. Shivakumara, R.P.S. Chakradhar, *Mater. Res. Bull.* **47**, 2085 (2012)
28. M. Salavati-Niasari, G. Hosseinzadeh, F. Davar, *J. Alloys Compd.* **509**, 134 (2011)
29. M. Salavati-Niasari, J. Javidi, F. Davar, A. Amini, *Fazl. J. Alloys Compd.* **503**, 500 (2010)
30. S.V. Eliseeva, J.C.G. Bünzli, *Chem. Soc. Rev.* **39**, 189 (2010)
31. J.C.G. Bünzli, *Chem. Rev.* **110**, 2729 (2010)
32. C.W. Jung, P. Jacobs, *Magn. Reson. Imaging* **13**, 661 (1995)
33. C.M. Sorensen, Magnetism, in *Nanoscale Materials in Chemistry*, ed. by K.J. Klabunde (Wiley, New York, 2001), pp. 215–216
34. F.A. Cotton, G. Wilkinson, *Advanced Inorganic Chemistry* (Wiley, New York, 1980), pp. 983–985
35. S. Yin, S. Aktia, M. Shinozaki, R. Li, T. Sato, *J. Mater. Sci.* **43**, 2234 (2008)
36. G. Wang, Z. Wang, Y. Zhang, G. Fei, L. Zhang, *Nanotechnology* **15**, 1307 (2004)
37. X.C. Song, Y.F. Zheng, Y. Wang, *Mater. Res. Bull.* **43**, 1106 (2008)
38. M. Rahimi-Nasrabadi, F. Ahmadi, M. Eghbali-Arani, *J. Mater. Sci. Mater. Electron.* **27**, 11873 (2016)
39. M. Rahimi-Nasrabadi, M. Behpour, A. Sobhani-Nasab, M. Rangraz Jeddy, *J. Mater. Sci. Mater. Electron.* **27**, 11691 (2016)
40. F. Ahmadi, M. Rahimi-Nasrabadi, A. Fosooni, M. Daneshmand, *J. Mater. Sci. Mater. Electron.* **27**, 9514 (2016)
41. S.M. Pourmortazavi, M. Taghdiri, N. Samimi, M. Rahimi-Nasrabadi, *Mater. Lett.* **121**, 5 (2014)
42. M. Rahimi-Nasrabadi, S.M. Pourmortazavi, M.R. Ganjali, S.S. Hajimirsadeghi, M.M. Zahedi, *J. Mol. Struct.* **1047**, 31 (2013)
43. M. Rahimi-Nasrabadi, S.M. Pourmortazavi, M. Khalilian-Shalamzari, S.S. Hajimirsadeghi, M.M. Zahedi, *Open Chem.* **11**, 1393 (2013)
44. S.M. Pourmortazavi, M. Rahimi-Nasrabadi, M. Khalilian-Shalamzari, H.R. Ghaeni, S.S. Hajimirsadeghi, *J. Inorg. Organomet. Polym. Mater.* **24**, 333 (2014)
45. M. Rahimi-Nasrabadi, S.M. Pourmortazavi, A.A. Davoudi-Dehaghani, S.S. Hajimirsadeghi, M.M. Zahedi, *Cryst. Eng. Comm.* **15**, 4077 (2013)
46. S.M. Pourmortazavi, M. Rahimi-Nasrabadi, S.S. Hajimirsadeghi, *J. Dispers. Sci. Technol.* **33**, 254 (2012)

47. M. Rahimi-Nasarabadi, F. Ahmadi, S. Hamdi, N. Eslami, K. Didehban, M.R. Ganjali, *J. Mol. Liq.* **216**, 814 (2016)
48. S.M. Pourmortazavi, S.S. Hajimirsadeghi, M. Rahimi-Nasarabadi, I. Koksari, *Synth. React. Inorg. Metal Org. Nano Metal Chem.* **42**, 746 (2012)
49. R.K. Roy, *A Primer on the Taguchi Method* (Van Nostrand Reinhold, New York, 1990)
50. P.J. Ross, *Taguchi Techniques for Quality Engineering* (McGraw-Hill, New York, 1988)